Mon. Not. R. astr. Soc. (1981) **197**, 513–527

H_2CO mapping toward DR21 and W58 (K3 # 50)

J. R. Forster *Radiosterrenwacht, Postbus 2, 7990 AA Dwingeloo, The Netherlands*

W. M. Goss *Kapteyn Astronomical Institute, Postbus 800, 9700 AV Groningen, The Netherlands*

H. R. Dickel *University of Illinois, 341 Astronomy Building, 1011 W. Springfield Avenue, Urbana, Illinois 61801, USA*

H. J. Habing *Sterrewacht, Huygens Laboratory, Postbus 9513, 2300 RA Leiden, The Netherlands*

Received 1981 February 28; in original form 1981 January 6

Summary. We have mapped the distribution of 4.8-GHz H_2CO absorption against the galactic H II regions DR21 and W58 (K3#50) with 8 arcsec resolution. Opacity variations on scales less than 18 arcsec (0.2 pc) are seen against the extended continuum emission toward DR21. Extreme variations are observed toward the various radio components in W58. The H_2CO equivalent width is 5.2 km s^{-1} in the direction of component C1; it is < 0.03 toward K3#50. The linewidths are comparable to single-dish values for both DR21 and W58. H_2 column densities derived from the H_2CO equivalent widths are compared to the visual extinction. Large variations in the apparent H_2CO/H_2 abundance ratio are derived for W58.

1 Introduction

For many reasons, large molecular clouds are expected to contain structure on scales less than a parsec. Some processes which naturally produce density condensations are internal and external shocks, intereactions with other clouds, and stellar winds. In clouds containing active star-forming regions, these processes may dominate the structure and evolution of the cloud. The character of density condensations, or clumps, in molecular clouds associated with H II regions is poorly understood. Their size, mass distribution, temperature and density are essentially unknown. Knowledge of their physical characteristics can, however, add important information about the structure of molecular clouds and the process of star formation.

Indirect evidence for small-scale density condensations is seen in the low filling-factors derived from observed isotopic line-ratios (*cf.* Frerking *et al.* 1980), anomalies in hyperfine spectra (*cf.* Matsakis *et al.* 1977) and observed optical depth ratios in several molecular line

transitions (*cf.* Evans *et al.* 1975). Molecules with high dipole moments, such as NH_3, CN and CS, give indications of the presence of a dense ($> 5 \times 10^4\,cm^{-3}$) component in warm molecular clouds (*cf.* Plambeck & Williams 1979; Little *et al.* 1980). Excessive line-broadening over the expected thermal values suggests that the line-emitting/absorbing regions possess substantial peculiar velocities. Direct evidence of non-uniformity in molecular clouds comes from large-scale mapping in CO and other molecular lines. The optically thick ^{12}CO line often exhibits spatial structure down to the resolution limit of the telescope. The optically thin ^{13}CO line, which is a better tracer of density than the ^{12}CO line, is less extended and sometimes reveals several compact cores embedded in the molecular cloud (Israel 1981).

Of course, the contraction of gas into stars is the ultimate example of density condensation. Early theories of star formation envisaged a smooth interstellar medium in which molecular clouds were precipitated by thermal and gravitational instabilities. Modern theories (Norman & Silk 1980) suggest a more dynamic evolution. Rather than being smooth, the ISM is composed of gaseous clumps. These clumps coagulate into large molecular clouds which subsequently produce massive stars. These stars then disperse the cloud by sweeping away material by radiation pressure and shock waves. One obvious observational check of this theory is to look for clumps in the material overlying regions of star formation. The following sections present evidence for the existence of such clumps in DR21, and attempt to derive some of their characteristics. Sizes and densities are calculated which depend on the abundance ratio and excitation conditions of the H_2CO molecule. The relative abundance of H_2CO is estimated by comparison with the optical extinction. Clump sizes are measured directly from maps of the opacity distribution in front of the H II regions. H_2CO observations in the direction of the W58 complex are also presented. These show larger variations in the H_2CO opacity toward the various compact and extended H II regions detected. Although some of the variation can be explained by line-of-sight effects, interesting anomalies occur toward the peculiar object K3#50 and the ultracompact H II region (component C1) associated with the 1720-MHz OH maser ON 3.

The use of aperture synthesis instruments for H_2CO absorption-line mapping was pioneered by Fomalont & Weliachew (1973). They obtained a spatial resolution of 40 arcsec at 4.8-GHz with the Owens Valley interferometer. Subsequent H_2CO work by Whiteoak, Rogstad & Lockhart (1974) was done with a spatial resolution of 20 arcsec and velocity resolution of $3\,km\,s^{-1}$. We have observed the 4.8-GHz H_2CO line in absorption with an angular resolution of 8 arcsec and a velocity resolution of $0.7\,km\,s^{-1}$. Aperture synthesis instruments are particularly suited for H_2CO absorption studies because the 6-cm line is usually cooled by collisions to below 2.7 K. Large-scale absorption against the 2.7 K background, which can strongly affect single-dish profiles, is filtered out by the interferometer. The purpose of these observations was to map the distribution of H_2CO optical depth in front of extended continuum-emission regions in order to determine the scale-size of opacity variations in the overlying molecular cloud.

2 Observations and data reduction

The Westerbork Synthesis Radio Telescope (WSRT) was used with a maximum baseline of 1440 m. The number of interferometers was 40, with grating rings at radial intervals of 5.6 arcmin in right ascension. The observing frequency was centred at the 1_{10}–1_{11} H_2CO line at 4829.66 MHz. Two orthogonal linear polarizations were averaged to form 31 frequency maps in total intensity. The velocity range is $19.4\,km\,s^{-1}$. The velocity resolution is $0.73\,km\,s^{-1}$, with $0.61\,km\,s^{-1}$ separation between frequency points. The synthesized beam is

8 arcsec FWHM in RA (8 arcsec/(sin Dec) in Dec) after tapering the uv data. The primary beam size is 10.8 arcmin. The system temperature was 120 K, giving an rms noise of 3 K in an individual channel map. The observations were obtained in 1978 May in two 12-hr periods.

The channel maps were made in the standard way. The uv data were weighted with a Gaussian taper which reached 0.25 at the longest baseline. The theoretical synthesized beam has maximum sidelobes of 5 per cent. During the observations, some of the telescopes were affected by temperature changes in the front-ends, which caused phase errors in the measured visibilities. An empirically derived correction was applied which accounts for most of the error, but the continuum maps have limited dynamic range (7 per cent after cleaning). However, to the extent that all channel maps are similarly affected, these errors cancel in forming optical depth. The channel maps were converted to optical depth by dividing by a continuum map (T_c) and taking the natural logarithm: $\tau = -\ln(T_j/T_c)$, where j refers to a particular channel. T_c was formed by averaging over channels which showed no H_2CO absorption.

The optical-depth maps were analysed by fitting Gaussians to the optical-depth profiles. Since the noise in the optical-depth maps is proportional to $1/T_c$, only positions where $T_c > T_{min}$ were analysed. The rms error in τ was thereby restricted to less than 0.03. In regions where the continuum brightness is greater than the cut-off, the rms error in τ is proportionately less. It should be pointed out that the optical-depth maps are not entirely free from dynamic-range effects. For channel maps with low absorption, dynamic-range distortion is nearly identical to that of the continuum map and therefore cancels in taking the ratio of the line to continuum. However, for channels having large absorption and hence low values of measured signal, the dynamic-range distortion in the line and continuum does not cancel. We have tried to account for this in our error estimation, and believe that it does not substantially alter the values derived or the conclusions.

3 Results

The H_2CO optical-depth profiles averaged over each quadrant in DR21 are shown in Fig. 1 along with the continuum map. The narrow, blended component at $-4\,km\,s^{-1}$ is also visible in the 2-cm spectrum of Evans *et al.* (1975). The distribution of H_2CO equivalent-width $W(=\int \tau dv)$ for the two main features at $-2\,km\,s^{-1}$ (integration range -6 to $+2\,km\,s^{-1}$) and $+8\,km\,s^{-1}$ (integration range $+5$ to $+10\,km\,s^{-1}$) is presented in Fig. 2. The variation of W over the area shown in Fig. 2 is about a factor of 2.5. Gaussian decomposition of the blended negative-velocity features at -4 and $-2\,km\,s^{-1}$ was attempted over the brightest part of the background source where the rms noise in the optical-depth maps is less than 0.01. The results of a three-component Gaussian fit to the line profiles are presented in Fig. 3. The three components have the nominal values and variations listed in Table 1. The estimated errors are given in parenthesis. These are based on the formal error in the Gaussian fit and are 1σ. Since the rms error depends on the line strength and the continuum intensity, a representative value is given. Values for the blend of the two negative-velocity features are also given. The variation in FWHM is probably not significant for the $-4\,km\,s^{-1}$ feature where it is heavily blended. There appears to be a slight tendency for the linewidths to increase with opacity. The $-4\,km\,s^{-1}$ feature shows the largest variation in both optical depth and linewidth. This feature and the one at $+8\,km\,s^{-1}$ have similar opacity distributions, and appear to be anti-correlated with the strong feature at $-2\,km\,s^{-1}$.

H_2CO optical-depth profiles toward five radio components in W58 are presented in Fig. 4, along with a schematic of the 6-cm continuum emission superposed on the ^{13}CO column

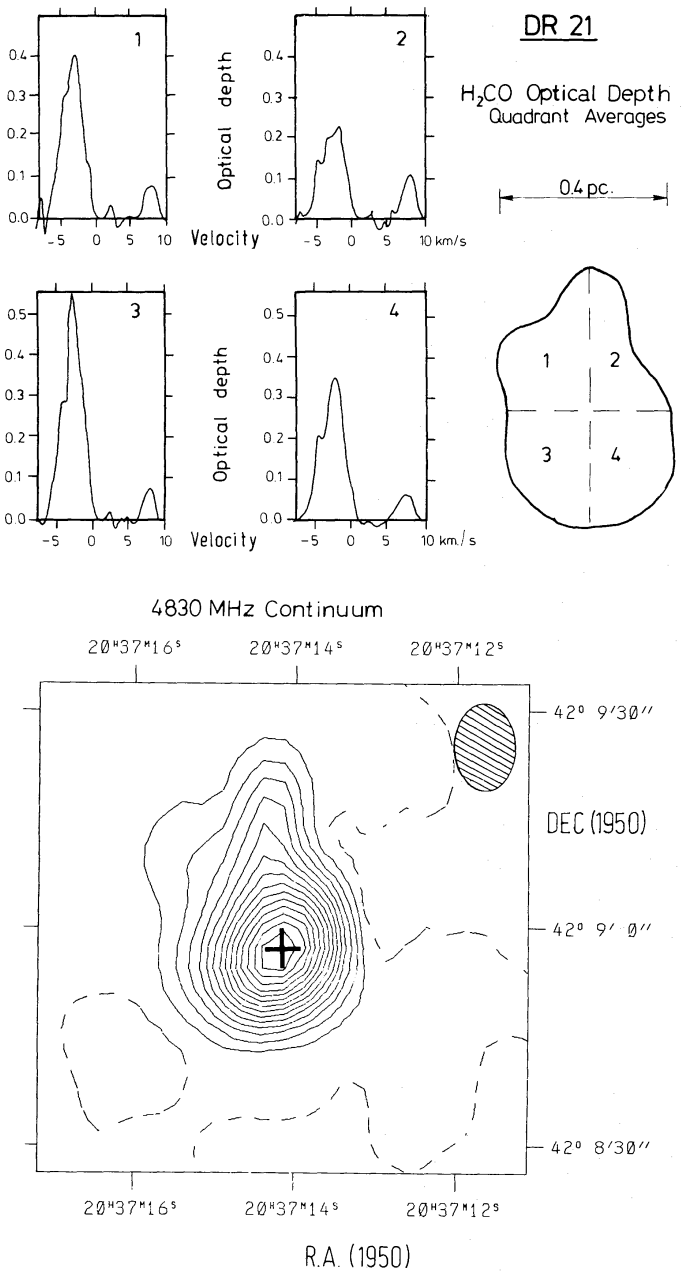

Figure 1. 6-cm H_2CO optical-depth profiles averaged over four quadrants in DR21. The contour interval of the continuum map is 250 mJy/beam. The shaded ellipse shows the half-power beam area. Velocity is with respect to the Local Standard of Rest.

Table 1. Range of values for H_2CO absorption features mapped against DR21.

Velocity (km s^{-1})	FWHM (km s^{-1})	Equivalent width (km s^{-1})
+ 7.9 to + 8.4 (0.2)	1.4 to 1.9 (0.4)	0.12 to 0.28 (0.06)
− 2.5 to − 1.8 (0.2)	2.5 to 3.1 (0.3)	0.55 to 1.76 (0.05)
− 4.7 to − 4.0 (0.2)	1.0 to 2.0 (0.4)	0.09 to 0.47 (0.06)
★ − 2.9 to − 2.2 (0.2)	2.6 to 4.1 (0.3)	0.85 to 1.82 (0.04)

★ Not the result of a Gaussian fit; parameters were directly measured for the − 4 km s^{-1}, − 2 km s^{-1} blend.

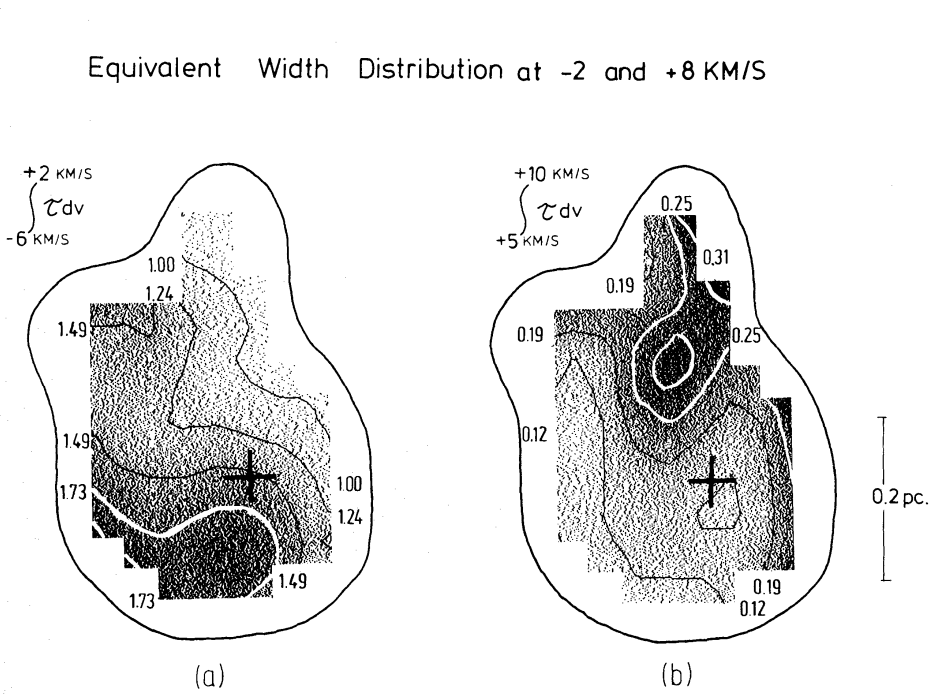

Figure 2. (a) The distribution of H_2CO equivalent width for the blended features at -4 and $-2\,km\,s^{-1}$ integrated from -6 to $+2\,km\,s^{-1}$. The units of equivalent width are $km\,s^{-1}$. (b) Equivalent width distribution of the $+8\,km\,s^{-1}$ feature integrated from $+5$ to $+10\,km\,s^{-1}$. Contour levels are marked on the figure. The cross marks the position of peak continuum intensity.

density map of Israel (1981). Profiles for components C1, C2 and A (K3#50) come from single points in the map, since they are unresolved with the 8 arcsec beam. Profiles for components B and D (NGC 6857) are averages obtained by summing over the extended continuum emission. The velocity, FWHM and equivalent width, W, obtained by Gaussian fitting to the optical-depth profiles are listed in Table 2. For the unresolved sources, the diameters measured by Harris (1975) are listed to give an idea of the linear extent of the absorbing region. These sizes are typically 2 to 4 times larger than the compact cores measured by Colley & Scott (1977) at 15 GHz. The rms errors in velocity, FWHM and W are given in parentheses. Our H_2CO results are in good agreement with the 100-m Effelsburg observations of van Gorkom *et al.* (1981) when smoothed to the same resolution.

The striking thing about this region is the large variation in H_2CO optical depth. The two brightest H II regions, K3#50 and C1, differ by more than two orders of magnitude in H_2CO equivalent width. C1 has a peak optical depth of 1.82 compared to 0.23 for C2. The absorption-line velocities are all the same, however, indicating that the lines definitely arise in the same cloud.

4 Interpretation

4.1 DR21

Velocity features similar to the H_2CO absorption lines are also seen in OH and CO spectra toward DR21 ($l = 82°$, $b = 3°$). These features apparently come from two separate molecular

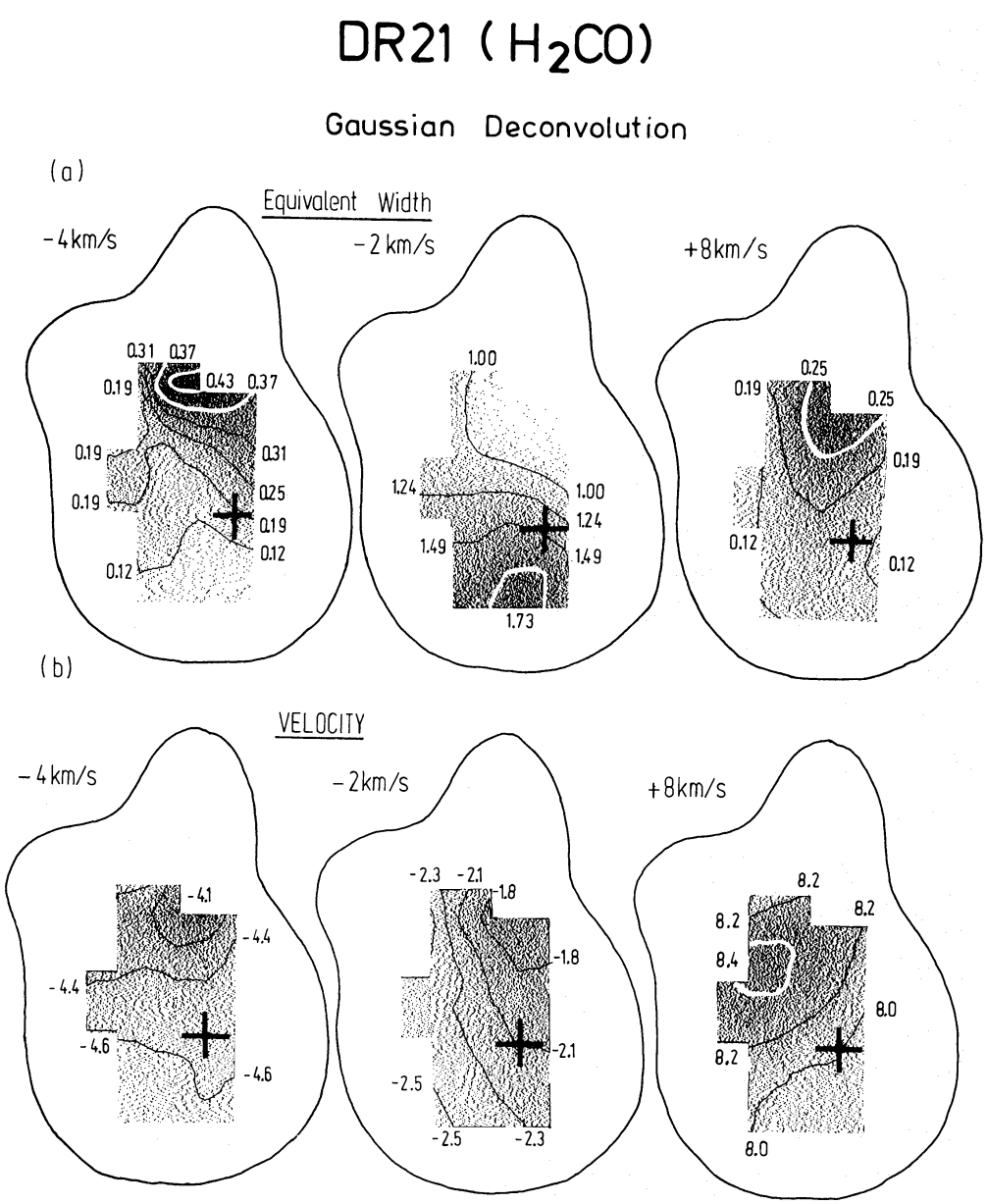

Figure 3. (a) The distribution of H_2CO equivalent width derived from Gaussian fitting to three components at -4, -2 and $+8$ km s^{-1}. Only points with rms uncertainties less than 0.01 in optical depth are plotted. The units are km s^{-1}. (b) Distribution of velocity for the three Gaussian components. Contour levels are labelled in km s^{-1}.

Table 2. H_2CO Absorption in W58 (K3#50).

Component	RA (1950) h m s	Dec (1950) ° ′ ″	Diameter (pc)★	Velocity (km s^{-1})	FWMH (km s^{-1})	W (km s^{-1})
C1 (ON 3)	19 59 58.5	33 25 49	0.22	−21.2 (0.1)	2.9 (0.1)	5.22 (0.10)
C2	59.7	25 53	0.14	−21.5 (0.2)	3.6 (0.4)	0.76 (0.08)
B	52.0	24 42	1.0	−21.6 (0.4)	5.6 (0.9)	0.35 (0.06)
D (NGC 6857)	51.8	23 04	1.5			<0.13
A (K3#50)	50.0	24 20	0.17			<0.03

★ The sizes for C1, C2 and A are from Harris (1975).

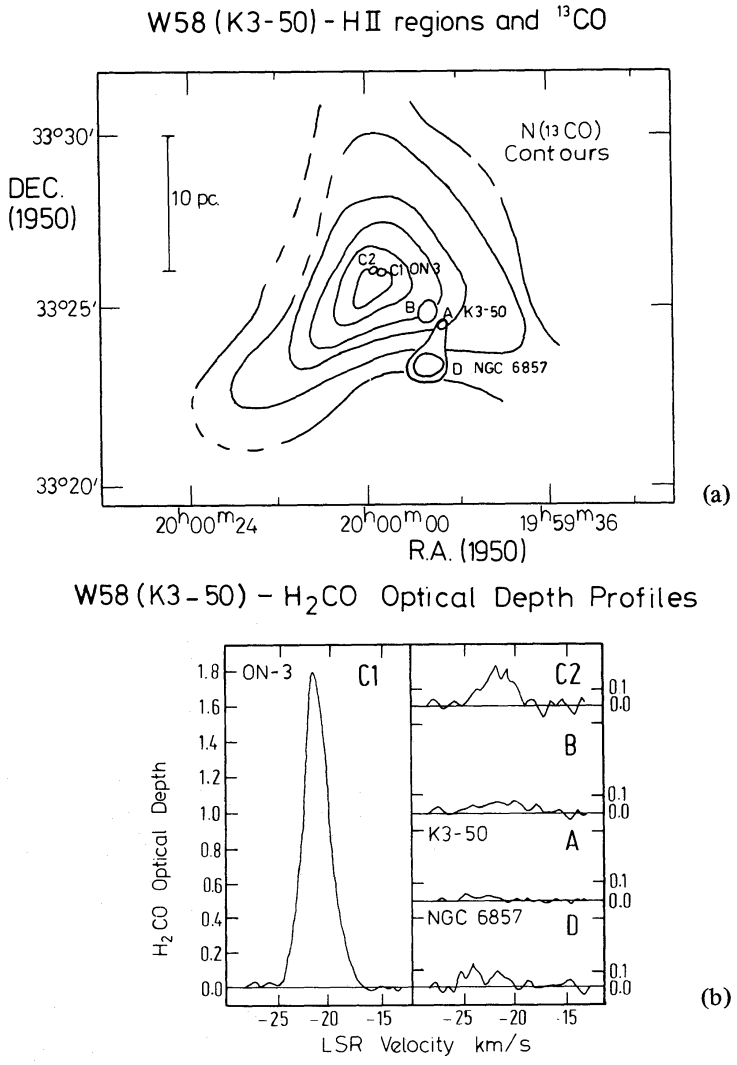

Figure 4. (a) Schematic diagram of the 6-cm radio continuum sources in W58 superposed on a ^{13}CO column-density map (Israel 1981). (b) H_2CO optical-depth profiles toward the radio continuum sources. All profiles have the same scale.

clouds (Dickel, Dickel & Wilson 1978, hereafter DDW). The $-3\,km\,s^{-1}$ cloud has a ^{12}CO peak near DR21, while the $+9\,km\,s^{-1}$ cloud peaks 18 arcmin to the north-west, near the weak continuum source W75(N). For an assumed distance of 2 kpc (DDW), both clouds extend over an area roughly 25 pc in diameter. Recognition of features common to both velocities led DDW to suggest that the two clouds are interacting. The H_2CO linewidths (FWHM) measured with the WSRT against DR21 are about $3\,km\,s^{-1}$ for the $-2\,km\,s^{-1}$ feature and $2\,km\,s^{-1}$ for the other two features. These are similar to the H_2CO halfwidths measured with single-dish telescopes. At a kinetic temperature of 35 K, thermal Doppler broadening accounts for only $0.23\,km\,s^{-1}$. The observed linewidths must therefore be due to turbulent or systematic motion of the gas. Some evidence for systematic motion is seen in the velocity fields. Two of the features show velocity changes of more than $0.7 \pm 0.3\,km\,s^{-1}$ over the area (0.4 pc) of Gaussian decomposition (Fig. 3b). In the case of the $-4\,km\,s^{-1}$ feature, there appears to be discontinuity of about $0.5\,km\,s^{-1}$ between the background velocity and the clump velocity. The $-2\,km\,s^{-1}$ feature varies smoothly in velocity and this variation does not appear correlated with the opacity distribution.

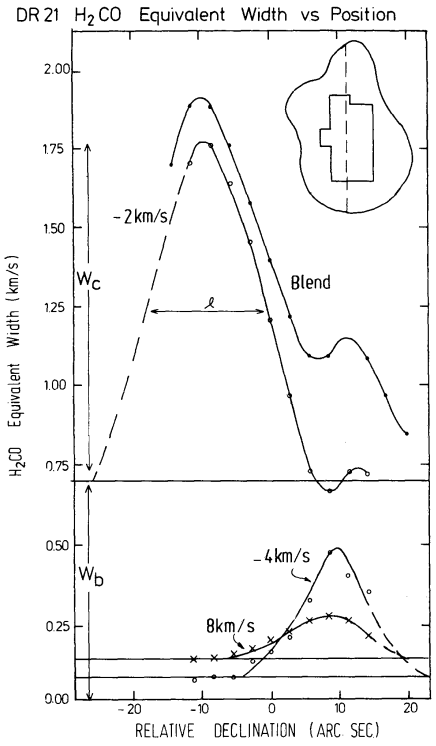

Figure 5. Plot of H_2CO equivalent width versus position for the three Gaussian components of Fig. 3(a). The blended (velocity range -6 to $+2\,km\,s^{-1}$) component of Fig. 2(a) is also plotted. The definitions of the parameters W_c, W_b and l are indicated for the $-2\,km\,s^{-1}$ feature. Spherical symmetry is assumed in estimating the scale-size l; extrapolation is indicated by dashed lines. The line along which points are taken (at RA = $20^h\,37^m\,14^s.5$ and Dec zero point = 42° 09′ 00″) is shown in the upper right-hand corner.

The H_2CO opacity toward DR21 clearly changes by factors of 2 to 3 over linear scales less than 0.2 pc (18 arcsec). If we identify these optical-depth enhancements with clumping in the molecular cloud, the volume density of a clump may be estimated from its equivalent width and its linear size, on the assumption of spherical symmetry. In Fig. 5, W is plotted versus declination for strips down the centre of the three distributions shown in Fig. 3(a). Where the clumps apparently extend beyond the edge of the continuum source (dashed lines), the size is estimated by assuming symmetry. The parameters obtained from each curve are (1) the 'background' equivalent width, W_b; (2) the 'clump' equivalent width, W_c, which is the peak increase in W at the clump over the background; and (3) the clump size, 1. In Fig. 5, W_b, W_c and l are indicated for the $-2\,km\,s^{-1}$ component. The background level, W_b, is indicated by a horizontal line for all three components.

The column density of molecules in the lower level (1_{11}) of the 6-cm transistion is given (Scoville, Solomon & Thaddeus 1972) by

$$N_{11} = 1.9 \times 10^{13} W [1-\exp(-0.232/T_{12})]^{-1} \qquad cm^{-2}.$$

The ratio of total formaldehyde to formaldehyde in the 1_{11} rotational state is about 2.6. This is calculated on the basis of the following assumptions: (1) a ratio of 3 to 1 for *ortho*-to-*para* formaldehyde, (2) excitation temperatures $T_{12} = 2.1\,K$, $T_{13} = T_{14} = 2.7\,K$, and (3) that levels above 2_{11} are unpopulated. The excitation temperatures are from Henkel, Walmsley & Wilson (1980), who determined T_{12} from an LVG radiation-transfer model using the H_2CO optical-depths measured for the 6-cm and 2-cm lines. These excitation temperatures are probably reasonable if the clump is not too near the H II region. Higher temperatures would

imply a greater population at the higher levels, as well as higher T_{12}. Both effects will cause an underestimate of the total H_2CO column density. In order to convert the formaldehyde density into a molecular hydrogen density, the abundance ratio $X(H_2CO) = H_2CO/H_2$ is needed. An average value may be estimated by comparing the H_2CO opacity with the measured optical extinction toward DR21. Righini-Cohen, Simon & Young (1979) derive an average A_V of 300 mag by comparing the [Ne II] emission-line strength at 12.8 μm with the values predicted from recombination-line theory using the radio flux densities and electron temperature from Harris (1973). These authors suggest that the true average extinction may be less by a factor of 2. They also measure Brackett α (4 μm) emission with an 11 arcsec beam at five positions in DR21 and obtain A_V ranging from 90 to > 130 mag toward the compact radio components. If we take an average A_V of 150 mag and $W = 1.6$ km s^{-1} (Fig. 2), we obtain $X(H_2CO) = 4 \times 10^{-9}$. For this calculation we have used the relation $N(H_2) = A_V \ 1.25 \times 10^{21}$ cm^{-2} (Jenkins & Savage 1974) and assumed $T_{12} = 2.1$ K. For DR21 we assume that $X(H_2CO)$ is the same for all lines of sight to the H II region. The justification for this is the small linear extent (0.5 pc) of the H II region. This assumption is not made for W58, where the H II regions are distributed throughout the volume of the 10-pc-diameter molecular cloud.

The hydrogen volume-densities calculated using this abundance ratio and the parameters measured from Fig. 5 are given in Table 3. It should be pointed out that the abundance of H_2CO relative to total hydrogen probably decreases with density. Wootten *et al.* (1978) find that $X(H_2CO)$ may vary by as much as three orders of magnitude in a comparison of various molecular clouds. According to their results, the abundance ratio derived above is appropriate for clouds with densities of about 2×10^4 cm^{-3}, but $X(H_2CO)$ may be 100 times smaller for densities greater than a few times 10^5 cm^{-3}. It is quite possible that $X(H_2CO)$ is lower in the clumps than in the ambient cloud. If $X(H_2CO)$ decreases with density, optical-depth changes due to density variations will tend to cancel. In fact, if $X(H_2CO)$ decreases faster than n^{-1}, the denser regions will have lower optical depths. A simple chemical scheme (Boland & de Jong 1981) suggests that $X(H_2CO)$ is roughly proportional to $n^{-1/2}$.

The hydrogen density derived by Henkel *et al.* in their LVG model is 1.3×10^5 cm^{-3}, assuming uniform coverage of the background source. A fractional coverage less than unity reduces the hydrogen density required in their model. In the NH_3 observations of Matsakis *et al.* (1977), the best fits to the data were obtained for $n > 5 \times 10^4$ cm^{-3} and a filling factor of 0.2. Observations of CN in this direction (Turner & Gammon 1975) yield a value of 2.5×10^4 cm^{-3}. An upper limit of 5×10^4 cm^{-3} was set by Liszt & Linke (1975) from CS observations. These numbers are in reasonable agreement with our values for the clump densities. Although all of these observations were made with single-dish antennas and sample a large volume of the cloud, emission from these molecules with high dipole moments is thought to be heavily weighted toward regions of enhanced density (Plambeck & Williams 1979).

Table 3. Hydrogen densities in background (n_b) and clumps (n_c) for DR21.

Velocity (km s^{-1})	W_c (km s^{-1})	W_b (km s^{-1})	l (pc)	$10^{-4} n_c$ (cm^{-3})	$10^{-3} n_b$ (cm^{-3})	n_c/n_b
+8.2	0.13	0.15	< 0.13	> 2.3	0.6	> 40
−2.1	1.06	0.70	0.17	14.1	2.6	50
−4.4	0.38	0.09	< 0.13	> 6.6	0.3	> 200
Blend	1.00★	0.88★	0.17	13.3	3.3	40

★ Integration range = −6 to +2 km s^{-1}.

The density enhancement in the clumps over the ambient density in the molecular cloud can be determined from the relation $n_c/n_b = (W_c/W_b) \times (L/l)$, where L is the path length through the molecular cloud to the H II region and it is assumed that T_{ex} is the same in the clump and the background. The model of DDW for the CO clouds at -3 and $+9\,km\,s^{-1}$ suggests a length of about 6 pc for the line of sight through each cloud. Using this distance for L, the derived density enhancement for the three clumps is given in Table 3. Since the densities are lower limits for the two unresolved clumps, the density enhancement is also a lower limit. Our results indicate that the clumps are at least 40 times more dense than the ambient cloud material. The ambient density of the two molecular clouds may be determined from the background equivalent width and the length L. These values are also given in Table 3. An average density of about $3 \times 10^3\,cm^{-3}$ is obtained for the $-3\,km\,s^{-1}$ cloud. This agrees with the density ($3 \times 10^3\,cm^{-3}$) derived by Plambeck & Williams (1979) from CO observations of the $-3\,km\,s^{-1}$ cloud in the direction of DR21 (OH). The density we derive for the $+8\,km\,s^{-1}$ cloud is about $6 \times 10^2\,cm^{-3}$.

In the above interpretation of the H_2CO opacity variations toward DR21 we have assumed that the excitation temperature is the same everywhere, and any changes in the optical depth are due to changes in the formaldehyde column density. However, variations in the excitation temperature T_{12} will have an affect on the measured optical depth opposite to changes in column density. The results of Evans *et al.* (1975) show that, over the range of densities indicated in Table 3 (5×10^2–$2 \times 10^5\,cm^{-3}$), T_{12} may vary by as much as a factor of 4. For warm clouds ($T_k > 20\,K$), collisions begin to raise the excitation temperature at about $3 \times 10^4\,cm^{-3}$. Thus the assumption of constant T_{12} may affect the derived densities by causing the density contrast between cloud and clump to appear lower than the true value. The measurement of scale sizes is probably not strongly affected by this assumption.

An important assumption regarding scale sizes is that the background source is at a constant distance behind the front edge of the absorbing cloud. If the background source is composed of components at different distances, or the absorbing cloud only partially covers the source, opacity variations may be observed which have nothing to do with internal structure in the cloud. From the CO maps of DDW it appears that the $-3\,km\,s^{-1}$ cloud varies smoothly on a scale much larger than the H II region. Both clouds have overall dimensions many times larger than DR21, so partial coverage seems unlikely. There remains the possibility that the radio components forming the background source are at different distances. This is certainly a possibility for DR21, since the high-resolution radio map of Harris contains at least 4 distinct components. It is possible that the northern component (D in Harris's notation, also coincident with the infrared source DR21 (N) of Wynn-Williams, Becklin & Neugebauer 1974) is near the front of the $-3\,km\,s^{-1}$ cloud. The recombination-line velocity (van Gorkom, in preparation) is more positive ($+3\,km\,s^{-1}$, as compared with $-3\,km\,s^{-1}$ toward the south) and the visual extinction (Righini-Cohen *et al.* 1979) is lower. If component D is in front of the cloud, the lower H_2CO opacity toward the north at $-2.1\,km\,s^{-1}$ may be explained without resorting to density variations. On the other hand, both the low H_2CO opacity and the low A_V could be due to a lower molecular hydrogen density in this direction. The H_2CO opacity variations at the other velocities occur where there are no compact components, and therefore must be due to structure within the absorbing cloud.

4.2 W58 (K3#50)

The W58 region ($l = 73°$, $b = 3°$) contains several compact and extended H II regions. Two of these are associated with the optical nebula NGC 6857 and the peculiar optical/infrared/radio object K3#50. Another is associated with the 1720-MHz OH maser ON 3. These H II

regions form a giant physical complex in Cygnus extending nearly a degree in the sky. A neutral hydrogen cloud covers an even larger area, with a peak near K3#50. The entire W58 region has been mapped in the radio continuum by Israel (1976), in ^{12}CO and ^{13}CO by Israel (1981), and in neutral hydrogen by Read (1980) and by Bridle & Kesteven (1970). High-resolution maps of the compact H II regions around K3#50 have been made at 5 GHz by Harris (1975) and at 15 GHz by Colley & Scott (1977). A 1-mm map has been made by Wynn-Williams *et al.* (1977) who also studied the infrared emission between 2 and 20 μm. Van Gorkom *et al.* (1981) have made H109α recombination-line observations with the Westerbock telescope and compare the velocity of the ionized gas with that of the neutral material. The distance of 8.7 kpc assumed by Israel (1976) will be used throughout.

As described by Israel (1981), the environment around K3#50 consists of a molecular cloud about 10 pc (4 arcmin) in extent, with a mean velocity of $-22\,km\,s^{-1}$ (Fig. 4). The average density of the cloud is about $2\times10^3\,cm^{-3}$, with a gradient increasing towards the east. An unresolved ridge of high CO column density delineates an area in the east where the CO cloud may be interacting with a larger H I cloud. This ridge coincides with a pair of ultracompact H II regions, one of which is associated with the OH maser ON 3. The other radio components, including K3#50, appear west of the ridge in regions of lower density. K3#50 is a peculiar optical object associated with a compact H II region and an infrared source. Wynn-Williams *et al.* (1977) measure a progressive position shift from radio to optical wavelengths, suggesting a large extinction gradient across the source. The two ultra-compact H II regions C1 and C2 are also infrared sources. Although both were easily detected at 20 μm, only C2 remains prominent at 2 μm. This large extinction at 2 μm led Wynn-Williams *et al.* to conclude that there are several hundred magnitudes of optical extinction in the direction of C1.

Using the relations described earlier for DR21, the 6-cm H_2CO column density N_{11} is obtained from the measured equivalent width. An excitation temperature of 1.7 has been used for this calculation (van Gorkom *et al.* 1981). Righini-Cohen *et al.* (1979) have measured the 4-μm Brackett α extinction toward components C1, C2 and A by comparison with the radio continuum flux density, and estimate the visual extinction in these directions. Israel (1976) has estimated the extinction toward component B from the non-appearance on the Palomar Sky Survey plates of an assumed exciting O star. The extinction toward the optical nebula NGC 6857 has been measured by Persson & Frogel (1974). We derive $X(H_2CO)$ from a comparison of our values for N_{11} and the measured values of A_V by assuming that the total hydrogen column density $N(H_2)$ is proportional to A_V and that the ratio of total formaldehyde to *ortho*-formaldehyde in the ground state is 2.6. The results are listed in Table 4.

Due to uncertainties in the optical extinction and excitation conditions, $X(H_2CO)$ may be in error by factors of 3 to 4. The low abundance derived toward K3#50 is surprising, however. If the formaldehyde abundance is 4×10^{-9} (as we found for DR21) in this

Table 4. Apparent formaldehyde abundance in W58 (K3#50).

Component	N_{11} ($10^{14}\,cm^{-2}$)	$N(H_2)$ ($10^{22}\,cm^{-2}$)	A_V* (mag)	$X(H_2CO)$ (10^{-9})
C1 (ON 3)	8	13	100	16
C2	1	3	25	10
B	0.5	>1	>10	<11
D (NGC 6857)	<0.2	0.5	4	<10
A (K3#50)	<0.04	2	17	< 0.5

*A_V for C1, C2 and A from Righini-Cohen *et al.* (1979), B from Israel (1976), and D from Persson & Frogel (1974).

direction, the optical extinction should not exceed 2 mag at the position of the radio peak. Even if the optical extinction is as low as 4 mag (Righini-Cohen *et al.* first estimated 4 mag for K3#50, then changed it to 17 mag using Colley & Scott's 15-GHz flux density), the formaldehyde abundance ratio toward K3#50 is still at least a factor of 5 less than toward component C.

Van Gorkom *et al.* (1981) interpret their H109α velocities, which range from $-31\,\mathrm{km\,s^{-1}}$ for K3#50 to $-16\,\mathrm{km\,s^{-1}}$ for component C, in terms of the blister model for H II regions. In this model the more negative recombination-line velocities are caused by H II regions on the side of the molecular cloud nearest the Earth, and the more positive velocities are produced by H II regions on the opposite side of the cloud. One H II region, component B, has a recombination-line velocity which is the same as the molecular cloud. This implies that it is embedded in the cloud, which is also suggested by its spherical shape (Israel 1976). Both the visual and H_2CO opacities give the trend predicted by the blister model, i.e. the opacity decreases as the recombination-line velocity decreases. This indicates that the variation in H_2CO opacity observed toward the different radio components in W58 can be generally accounted for by varying depths within the molecular cloud. If we assume that the molecular cloud has uniform volume density n, the thickness of the absorbing layer in a particular direction can be calculated from the ratio $N(H_2)/n(H_2)$. If we let $n(H_2) = 3\times10^3\,\mathrm{cm^{-3}}$, as suggested by the ambient cloud density derived toward DR21, the absorbing layer thickness in pc is approximately 13, 3, > 1, 0.5, and 2 for C1, C2, B, D, and A respectively. These values are consistent with the observed size (10 pc) of the $-22\,\mathrm{km\,s^{-1}}$ cloud. If the same method is applied using the H_2CO column density to calculate $N(H_2)$ and assuming that $X(H_2CO) = 4\times10^{-9}$ everywhere, the derived depths in pc are about 55, 7, 4, < 1.5 and < 0.3. These are generally 2 to 3 times larger than the thickness implied by the visual extinction, and probably mean that the average formaldehyde abundance ratio is a few times greater than 4×10^{-9}, as indicated in Table 4.

Significant variations in the apparent formaldehyde abundance ratio toward the radio components in W58 are indicated in Table 4. An apparent variation in $X(H_2CO)$ can be caused by many things, however. Different excitation conditions, absorption on to grains, and various chemical processes tend to make the apparent formaldehyde abundance a complicated function of temperature, density, cosmic-ray abundance and chemical composition. Because of this, it is difficult to distinguish apparent variations in $X(H_2CO)$ from real changes in the relative formaldehyde abundance. The low optical depth measured toward K3#50 may not be incompatible with the Wynn-Williams *et al.* (1977) interpetation of a large extinction-gradient, for example, if the temperature of the obscuring gas and dust is substantially higher than 30 K. Similarly, the high apparent abundance toward C1 may also be caused by temperature and density effects. One such effect was discussed by Harris (1975) with regard to K3#50, but it might be more applicable to C1. The mechanism proposed causes an apparent reduction in A_V toward compact sources surrounded by dense layers of dust. In travelling through a dense dust layer, optical photons scattered out of the line of sight have a high probability of being scattered back again, provided the telescope beam includes the whole dust shell. This reduces the apparent optical extinction for a given column density of dust. Since scattering is not important in the collisionally cooled 6-cm H_2CO line, the formaldehyde opacity will not be affected. The result is a high apparent formaldehyde abundance. Of course, this will not explain K3#50, which has a low apparent formaldehyde abundance. The mechanism was originally proposed to explain the peculiar extinction observed toward K3#50 (Persson & Frogel 1974). This explanation no longer seems necessary in view of the position shifts measured by Wynn-Williams *et al.*, but the optical extinction of K3#50 is still anomalous according to our H_2CO results.

5 Discussion

If we are correct in interpreting the H_2CO optical-depth variations toward DR21 as clumps of dense material in the molecular cloud, we can make the following statements. The clumps have a diameter of 0.2 pc or less, cover less than 20 per cent of the region of continuum emission, and are at least 40 times more dense than the surrounding gas. The absorption lines produced in a clump are not substantially narrower than the lines observed in the surrounding gas. This last implies that the broad absorption-lines seen with single-dish telescopes are not due to peculiar motions of cloudlets which themselves have thermal halfwidths, unless the scale size of these cloudlets is much smaller than 0.1 pc. Since the clumps produce broad absorption-lines (2–3 km s^{-1}), whereas the thermal halfwidth for H_2CO at 35 K is 0.23 km s^{-1}, we conclude that the H_2CO molecules are probably in turbulent motion. In order to account for the observed linewidths, an rms velocity of about 1 km s^{-1} is required.

From the size and density of the clumps, the mass and energy can be calculated. With a radius of 0.1 pc and density of 10^5 cm^{-3}, the clump contains about $20 M_\odot$. The total gravitational energy is $GM^2/r = 4 \times 10^{44}$ erg. The total internal kinetic energy is $1/2 Mv^2$, where M is the total clump mass and v is the rms velocity (thermal plus turbulent) of the gas. For v = 1 km s^{-1} the internal kinetic energy is 2×10^{44} erg. If the same amount of energy is present in magnetic fields, the field strength is 150 μG. Since the total internal and gravitational energies are comparable, the clump may be stable against further collapse. Following Javanaud (1980), the critical radius for a cloud of M solar masses and kinetic temperature T is $R_c = 0.44 M/T$ pc. With $M = 20$ and $T = 35$, $R_c = 0.25$ pc. This would indicate that the critical radius has been reached and the clump is collapsing. However, only thermal pressure has been accounted for in this calculation (the rms thermal velocity for H_2 molecules is 0.4 km s^{-1}). As seen above, additional internal energy in the form of turbulence may provide enough pressure to stop the collapse.

Unfortunately, we have no direct information on the location of the clumps with respect to the H II region. Some arguments for a close association with the H II region can be made, nevertheless. The high-resolution continuum map of Harris (1975) shows four compact components contained within an extended envelope of ionized gas. The brightest of these, component C, lies just north of the -2 km s^{-1} clump. Components B and D lie on opposite edges of the +8 km s^{-1} clump (Fig. 2). It may be that the compact continuum-components are bounded in these directions by the clumps. Recombination-line observations made with the WRST (van Gorkom, in preparation) indicate the presence of a dense ($> 10^5$ cm^{-3}) component in the ionized gas corresponding to the compact sources of Harris. The agreement in density for the clumps and the dense ionized gas lends support for a close association, as do the similar velocities.

As suggested by DDW, and also indicated in our H_2CO observations, the clumping in DR21 may be related to an interaction between two large molecular clouds. We have already mentioned that the opacity of the -2 km s^{-1} feature is anti-correlated with the +8 km s^{-1} feature. If this is not purely coincidental, it implies that the clumps are physically associated. An even more remarkable similarity exists between the +8 and the -4 km s^{-1} clumps. Both are unresolved and positionally coincident within the error of measurement. They also have similar linewidths, which are significantly less than that of the -2 km s^{-1} feature. These correlations are strongly suggestive of the cloud–cloud collision proposed by DDW, although the details of the interaction are unclear. Since DR21 is also assumed to be located in the interaction zone, this is further support for a close association with the H II region.

Of course, there is the possibility that the clumps are not related to the H II region. They could be random clumps in the molecular cloud which just happen to lie along the line of sight. The clump and interclump densities derived for DR21 are in agreement with the values

suggested by Norman & Silk (1980) in their T Tauri wind model. The broad absorption lines seen toward the clumps are also consistent with this model.

The average formaldehyde abundance ratio $X(H_2CO)$ derived for DR21 is about 4×10^{-9}. In W58, $X(H_2CO)$ is at least eight times smaller than this toward K3#50, while toward component C1 it is four times larger. Although the uncertainty in $X(H_2CO)$ is large, these differences are significant. Since the *apparent* relative formaldehyde abundance depends strongly on the excitation of the observed transition, these variations may reflect changing physical conditions rather than actual chemical abundance variations. For the two sources which show the greatest deviation, K3#50 and component C1, there is evidence of locally dense gas and dust. The large extinction-gradient associated with K3#50 has already been discussed. The presence of OH and H_2O masers near C1 indicates that this source may be surrounded by a dense cocoon, or pieces of one. The close proximity of component C2, which has far less optical extinction, puts an upper limit of about 1 pc on the extent of the obscuring matter near C1, if C1 and C2 are both located at the back edge of the molecular cloud. Recombination-line observations at higher spatial resolution are required to determine whether or not this is the case.

We have interpreted the observed variations in the formaldehyde optical depth as representing the clumpy nature of the interstellar medium. The observed parameters of these clumps in DR21 ($n(H_2) = 10^5\,cm^{-3}$, $l < 0.2$ pc, and fractional coverage of 20 per cent) agree with those inferred from the analysis of the anomalous ammonia spectra by Matsakis *et al.* (1977). As well as observing the clumps, we have found two additional, rather unexpected results which have significant implications for the determination of abundances of high-excitation molecules if their emission arises primarily from within these dense clumps.

First, DR21 and W58 belong to the class of warm, dense clouds containing embedded excitation sources for which Wootten *et al.* (1978) derive a typical formaldehyde abundance ratio of 10^{-11}; the abundance determined from the WSRT data is, however, more representative of dark clouds, where $X(H_2CO)$ is about 10^{-9}. Secondly, one might have expected the small clumps to have narrow linewidths (near the thermal value) so that the parameter $\Delta v/l$ would be $2.5\,km\,s^{-1}\,pc^{-1}$ as observed by the lower-resolution 1 to 2 arcmin beams of single dishes, where l is 1–3 pc and Δv is 3–5 $km\,s^{-1}$. Instead we have found that the linewidths remain large in the clumps, so that $\Delta v/l$ is 10–20 $km\,s^{-1}\,pc^{-1}$ instead of $2.5\,km\,s^{-1}\,pc^{-1}$. Thus we emphasize that, even within these small clumps, there is some unexplained broadening mechanism for the lines; it cannot merely be random motions between clumps.

The parameter $\Delta v/l$ is used in the large-velocity-gradient approximation is radiative-transfer calculations for deriving molecular abundances. Thus the effect of the smaller fractional coverage and larger velocity-gradients found here is to raise the molecular abundances over those determined assuming a uniform cloud model. Wootten *et al.* (1978) have acknowledged that a fractional coverage of 50 per cent due to clumping would raise their derived abundances by an average factor of 5 and up to 14. An additional increase of 4 to 8 results from the higher velocity-gradient which we have found. Thus much of the apparent depletion measured by Wootten *et al.* may well be accounted for by these two effects. In future determinations of molecular abundances, it is therefore important to consider models which include clumping.

6 Summary and conclusions

We have interpreted H_2CO opacity variations seen in absorption against DR21 as condensations or 'clumps' in the surrounding molecular cloud. One clumps has a size of about 0.2 pc; two others are smaller than 0.1 pc. The 0.2-pc clump has an average density of $10^5\,cm^{-3}$ and is contained in a cloud of density $3 \times 10^3\,cm^{-3}$. The mass of the clump is about

$20 M_\odot$. The halfwidths of the absorption lines in the clumps are not significantly different from the halfwidths in the ambient molecular cloud. Line broadening is probably due in part to turbulent motion of the gas on scales much smaller than 0.1 pc.

The H_2CO absorption lines toward the various H II regions in W58 show large variations in optical depth. These variations are in general agreement with the optical extinction, and with the line-of-sight depth through the absorbing cloud predicted by the blister model. The apparent formaldehyde abundance-ratio, H_2CO/H_2, is not the same toward all radio components. Component C1, which has an associated 1720-MHz OH maser, shows an anomalously high abundance, while component A, associated with the peculiar object K3#50, shows an anomalously low abundance.

Acknowledgments

We acknowledge many useful discussions with Wilfried Boland, Jacqueline van Gorkom and Teije de Jong. We are grateful to J. van Gorkom for communicating results prior to publication. The data reduction was done at the Computing Center of the University of Groningen, and we thank many people who helped develop the GIPSY system. The Westerbork Synthesis Radio Telescope is operated by the Netherlands Foundation for Radio Astronomy with the financial support of the Netherlands Organization for the Advancement of Pure Research (ZWO).

References

Boland, W. & de Jong, T., 1981. *Astr. Astrophys.*, in press.
Bridle, A. H. & Kesteven, M. J. L., 1970. *Astr. J.*, **75**, 902.
Colley, D. & Scott, P. F., 1977. *Mon. Not. R. astr. Soc.*, **181**, 703.
Dickel, J. R., Dickel, H. R. & Wilson, W. J., 1978. *Astrophys. J.*, **223**, 840.
Evans, N. J. II, Zuckerman, B., Morris, G. & Sato, T., 1975. *Astrophys. J.*, **196**, 433.
Fomalont, E. B. & Weliachew, L., 1973. *Astrophys. J.*, **181**, 781.
Frerking, M. A., Wilson, R. W., Linke, R. A. & Wannier, P. G., 1980. *Astrophys. J.*, **240**, 65.
Harris, S., 1973. *Mon. Not. R. astr. Soc.*, **162**, 5P.
Harris, S., 1975. *Mon. Not. R. astr. Soc.*, **170**, 139.
Henkel, C., Walmsley, C. M. & Wilson, T. L., 1980. *Astr. Astrophys.*, **82**, 41.
Israel, F. P., 1976. *Astr. Astrophys.*, **48**, 193.
Israel, F. P., 1981. *Astrophys. J.*, in press.
Javanaud, C., 1980. *Mon. Not. R. astr. Soc.*, **190**, 487.
Jenkins, E. B. & Savage, B. D., 1974. *Astrophys. J.*, **187**, 243.
Liszt, H. S. & Linke, R. A., 1975. *Astrophys. J.*, **196**, 709.
Little, L. T., Brown, A. T., Macdonald, G. H., Riley, P. W. & Matheson, D. N., 1980. *Mon. Not. R. astr. Soc.*, **193**, 115.
Matsakis, D. N., Brandshaft, D., Chui, M. F., Cheung, A. C., Yngvesson, K. S., Cardiasmenos, A. G., Shanley, J. F. & Ho, P. T. P., 1977. *Astrophys. J.*, **214**, L67.
Norman, C. A. & Silk, J., 1980. *Astrophys. J.*, **238**, 158.
Persson, S. E. & Frogel, J. A., 1974. *Astrophys. J.*, **188**, 523.
Plambeck, R. L. & Williams, D. R. W., 1979. *Astrophys. J.*, **227**, L43.
Read, P. L., 1980. *Mon. Not. R. astr. Soc.*, **192**, 11.
Righini-Cohen, G., Simon, M. & Young, E. T., 1979. *Astrophys. J.*, **232**, 782.
Scoville, N. Z., Solomon, P. M. & Thaddeus, P., 1972. *Astrophys. J.*, **172**, 335.
Turner, B. E. & Gammon, R. H., 1975. *Astrophys. J.*, **198**, 71.
van Gorkom, J. H., Shaver, P. A., Pottash, S. R., Blair, G. N. & Matthews, H. E., 1981. *Astr. Astrophys.*, **94**, 259.
Whiteoak, J. B., Rogstad, D. H. & Lockhart, I. A., 1974. *Astr. Astrophys.*, **36**, 254.
Wootten, A., Evans, N. J. II, Snell, R. & Vanden Bout, P., 1978. *Astrophys. J.*, **225**, L143.
Wynn-Williams, C. G., Becklin, E. E. & Neugebauer, G., 1974. *Astrophys. J.*, **187**, 473.
Wynn-Williams, C. G., Becklin, E. E., Matthews, K., Neugebauer, G. & Werner, M. W., 1977. *Astrophys. J.*, **179**, 255.